Expansion behavior and pair correlations in continuously excited Rydberg systems

N. Thaicharoen, S. A. Miller, and G. Raithel

Phys. Rev. A **98**, 023402 — Published 3 August 2018

DOI: 10.1103/PhysRevA.98.023402

Expansion behavior and pair correlations in continuously excited Rydberg systems

N. Thaicharoen*,†, S. A. Miller††, and G. Raithel
Department of Physics, University of Michigan, Ann Arbor, Michigan 48109, USA
(Dated: May 29, 2018)

We study cumulative excitation of Rydberg atoms in blockaded and facilitated regimes. In order to observe the evolution of the system into a steady state, we employ excitation durations extending to longer than the kinetic time scale and the Rydberg-atom lifetime. Despite of the presence of strong van der Waals repulsion, the most probable separation between atoms remains fixed due to the continual Rydberg excitation. This indicates that the time scale on which facilitated excitation replenishes the expanding Rydberg-atom cloud is faster than the van der Waals expansion time scale. The cloud expansion velocities are observed to be slower than the terminal velocity of Rydberg-atom pairs prepared at the facilitation radius and subject to binary van der Waals interaction. Atom statistics in the facilitated regime show bimodal Poissonian distributions, an observation we attribute to the statistical nature of the facilitation process. One peak is due to facilitation avalanches that produce many Rydberg atoms, and the other reflects cases in which the facilitation does not gain traction.

I. INTRODUCTION

Recently there have been numerous studies of many-body Rydberg atom systems prepared from laser-cooled atom clouds [1–3]. Most of these investigations have been performed in a manner in which the Rydberg-atom sample is initially prepared using optical pulses that are short compared to other time scales of the system, and the subsequent dynamics are studied. A complementary case of considerable interest is if and how a continuously replenished Rydberg atom system, which has a variety of decay and collision channels and whose constituents are subject to strong interatomic forces, approaches a steady state. This becomes particularly relevant when the time scale of the optical excitation exceeds the radiative decay time and/or other kinematic and collisional time scales of the atoms. Several studies show that the Rydberg-atom system passes through a phase transition [4, 5] from cold gas phase to crystal [6–8] or aggregate phase [9–11]. To understand the underlying mechanisms, several calculations have been performed to simulate the initialization of the Rydberg-atom sample using rate equations [12, 13], a hybrid model [14], a mean-field approximation [15], and the exact Hamiltonian [16]. The number statistics of the Rydberg atoms [13, 17] and thermodynamic properties [18] have been used to establish that the system reaches a steady state.

In previous work, it has been observed that the repulsive van der Waals interaction between Rydberg atoms leads to an expansion of the Rydberg atom cloud [19]. It has been predicted [20] and observed [21] that the interacting entities subject to the van der Waals force are individual atoms, not superatoms (which are much heavier than individual atoms); hence the pair-wise expansion dynamics are relatively fast. In related work, effects of the Rydberg-atom excitation blockade and facilitated excitation [9–11] due to the van der Waals interaction have been investigated using atom counting statistics, including the Mandel Q-parameter [22], moments up to third order [10], as well as bimodal distributions [23].

In this work, we use spatial images of Rydberg-atom ensembles with submicron resolution [24, 25] to investigate Rydberg many-body quantum systems. In order to study the evolution of the systems, we vary the Rydberg excitation duration up to 320 μs. This timescale is longer than the timescale of converting van-der-Waals potential energy into kinetic energy [19, 21], and longer than the decay time of the Rydberg atoms (≈ 200 μs in this work). In the experiment we perform measurements of the spatial pair correlation functions, the overall expansion of the Rydberg-atom clouds, and the atom counting statistics. The experiment is performed using on-resonant and off-resonant excitation of the Rydberg state. This allows us to study the evolution in both the blockaded and the facilitated regimes, respectively.

II. EXPERIMENTAL SETUP

We prepare cold ^{85}Rb atoms in a magneto-optical trap at a density of $\gtrsim 10^{10}$ cm^{-3} and a temperature of ~ 100 μK. The atoms in the $5S_{1/2}$ state are subject to two-photon Rydberg excitation into the $70S_{1/2}$ state by simultaneously applying 780- and 480-nm excitation laser pulses with $\approx$1 GHz red-detuning from the $5P_{3/2}$ intermediate state. The chosen detunings Δ of the Rydberg state with respect to the two-photon resonance are 0 and 4 MHz. The 780-nm laser has a Gaussian beam parameter $w_0 = 0.75$ mm and a power of ~ 600 μW. The 480-nm laser has a $w_0 \approx 8$ μm and a power of 1.6 mW. The 480-nm beam forms an angle of approximately 70° with the 780-nm beam. The beams are linearly polarized along the same direction, and the two-photon Rabi frequency for Rydberg excitation at the beam centers is 60 kHz. We use excitation pulse durations of 5, 10, 20, 40, 80, 160, or 320 μs. During Rydberg-atom excitation, the static electric field is compensated to less than $\approx$ 20 mV/cm. Immediately after the excitation pulse, Rydberg atoms are ionized by application of a positive high voltage of 1600 V to a tip imaging probe (TIP). The ionization electric field at the atom location amounts to 6 kV/cm, which is sufficient to ionize Rydberg atoms as low as $19S$. Therefore all Rydberg atoms are detected.

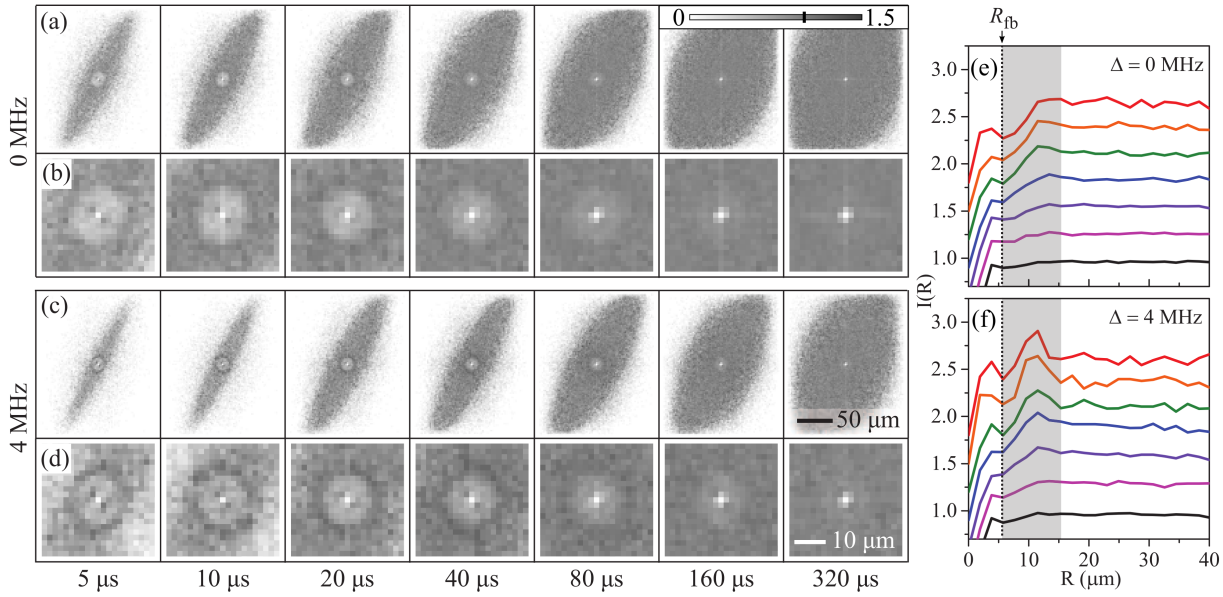

FIG. 1. Experimental pair correlation images for the indicated excitation pulse durations for $\Delta = 0$ (a, b) and $\Delta = 4$ MHz (c, d). (b) and (d) are enlarged versions of (a) and (c), respectively, to show the spatial pattern of the pair correlation enhancement ring. The linear grayscale ranges from 0 (white) to 1.5 (dark gray), where values of 1 (indicated by the black line on the grayscale bar), <1, and >1 indicate no correlation, anti-correlation, and positive correlation, respectively. The pattern near the center of each image is an experimental artifact due to ion feedback (see text). (e) Angular integrals $I(R)$ of the pair correlation images for $\Delta = 0$ for pulse duration 5 μs to 320 μs (from top to bottom). (f) same as (e) but for $\Delta = 4$ MHz. The numbers on the y axis are for the bottom (black) curve. For clarity, the other curves are shifted up in equidistant intervals of 0.3.

Further, since the rise time of the high-voltage pulse is on the order of ten nanoseconds, the field ionization is practically instantaneous. Ions are accelerated by the TIP electric field towards a microchannel plate (MCP). The excitation region is about 500 μm above the TIP, resulting in a magnification of 100±10. The ionization-pulse parameters are kept fixed, in order to maintain a constant experimental magnification ratio. Every detected ion results in a blip produced by the MCP-phosphor detector assembly, which reveals the center-of-mass position of its parent Rydberg atom at the time of ionization. We take 10000 images for each data set using a CCD camera. Using a peak-detection algorithm [25], we extract the total number of detected ions and their impact positions for each image. We then perform pair-correlation measurements, atom-cloud expansion studies, and atom-statistics analysis. Further details about the setup, detection, and processing are provided in [21, 26].

III. PAIR CORRELATION IMAGES AND ANGULAR INTEGRAL CURVES

The dynamics of the continuously excited Rydberg-atom samples lead to short-range structures, which become manifest in nearest-neighbor distributions and pair correlation functions, as well as an overall van der Waals-pressure-driven expansion dynamics. The spatial evolution is accompanied by decay and internal-state population redistribution of the Rydberg atoms as well as the continued production of new Rydberg atoms. The time scale over which the overall distribution of the Rydberg atoms in center-of-mass phase space and internal-state space approaches steady-state is longer than the radiative lifetime of the atoms. We first focus on short-range structure by calculating spatial pair correlation images using the 5000 records with the highest ion numbers. Each pair correlation image is normalized such that at large distances it approaches the value of one. The resulting pair correlation images for the selected excitation pulse durations for the $70S_{1/2}$ state for two laser detunings are shown in Figs. 1(a-d). Figures 1(a) and (c) show the pair correlation of the system. The enlarged images in Figs. 1(b) and (d) provide detailed information about the enhanced pair correlation (dark rings) and the blockade region (light-colored regions inside the dark rings).

At any time during the (long) excitation pulse, the ongoing continual excitation occurs within a sample of an evolved cloud of Rydberg atoms that have been excited at an earlier time, and that typically has expanded considerably due to the atoms' initial kinetic energies and van der Waals pressure. The excitation occurs within a volume given by the laser-beam size, which tends to be smaller than the extent of the evolved Rydberg-atom cloud. For the $\Delta = 0$ case, the excitation blockade results in suppression of Rydberg atoms with a separation less than the blockade radius $R_b = (C_6/\delta_L)^{1/6}$, where $C_6 = 5.77 \times 10^{-58}$ Jm^6 is the van der Waals interaction coefficient for the 70S state [27] and $\delta_L = 4 \pm 2$ MHz is the laser linewidth. This effect leads to the blockade region [25, 28] that is seen in Fig. 1(b) (light region at

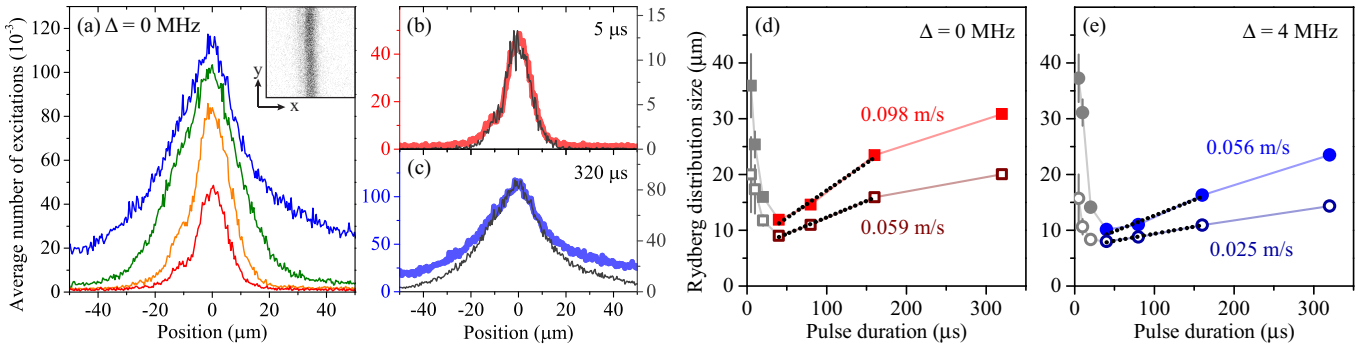

FIG. 2. (a) Rydberg atom cloud distributions at pulse durations 5, 20, 80, and 320 μs (inside to outside). The inset shows the sum of the 10000 images of the atom distribution taken at pulse duration 5 μs. In (b) and (c) we show the total distribution (thick line) versus the distribution that contains only pair-correlated atoms (thin line) for pulse durations 5 and 320 μs, respectively. The pair-correlated distributions are scaled to match the height of the total distributions. (d, e) Standard deviation σ_B of the total atom distributions (filled symbols) and pair-correlated atom distributions (hollow symbols) obtained from double-Gaussian fits to data for $\Delta = 0$ and $\Delta = 4$ MHz, respectively. Dotted lines are linear fits (over a limited time range), which yield the expansion velocities of the clouds. Gray symbols are neglected (see text for details).

the center of the images with a radius $\lesssim 10$ μm). A small fraction of atoms exhibits a weak "anti-blockade", *i.e.*, they are pair-correlated. This is evidenced by a low-visibility enhancement ring with a radius R_p of ~ 10 μm (the degree of correlation enhancement and the blockade radius depend on the laser linewidth and excitation geometry). The visibility of the blockade region is given by the contrast between the inside and outside region of the blockade region; it diminishes as a function of excitation duration. This is mostly due to the fact that we are looking at a 2-dimensional projection of a 3-dimensional atom cloud, whose extent along the direction of sight increases as a function of time. For $\Delta = 4$ MHz, pair or facilitated excitations usually occur when the laser detuning matches the van der Waals interaction. In this case, the separation between two Rydberg atoms is well defined [9, 11, 21, 26]. This leads to a strong enhancement ring that has a significantly higher visibility and smaller R_p than the one in the $\Delta = 0$ case. In both cases $\Delta = 0$ and $\Delta = 4$ MHz, with increasing excitation pulse duration R_p remains the same. This is because the time scale at which new Rydberg atoms are added to the expanding cloud (π-pulse duration ~ 8 μs) is much shorter than the van der Waals expansion timescale (~ 20 μs) [21]. This means that Rydberg atoms that are generated early-on during the excitation pulse repel and move away from each other, because of the van der Waals force, new Rydberg atoms are excited within the gaps that appear in the expanding Rydberg-atom cloud. The continual refilling of the gaps in the expanding sample with Rydberg atoms proceeds in a manner so as to maintain a relatively fixed value of R_p. Hence, the correlation distance R_p observed in the evolved, longer-time pair-correlation data tends to be the same as the R_p-value observed in the case of short excitation pulse duration (5 μs).

To quantitatively determine the enhancement radius R_p, we calculate the angular averages of the pair correlation images, $I(R)$. The $I(R)$ curves, displayed in Figs. 1(e, f) for both detuning cases, also show that R_p does not depend on time. The peak position of the $I(R)$ curve in the gray region represents R_p. Inspection of Fig. 1(e, f) shows that $R_p \approx 13$ μm for $\Delta = 0$ and $R_p \approx 11$ μm for $\Delta = 4$ MHz. The values for R_p have an uncertainty of about 2 μm due to the uncertainty in the magnification calibration. Also, the laser detuning Δ carries an uncertainty of about 2 MHz. Figures 1(e, f) further affirm that R_p does not significantly change as a function of excitation duration.

The overall growth of the pair correlation images in Fig. 1 as a function of time reflects the expansion of the cloud driven by the van der Waals pressure, which results in an increasing likelihood of accidental long-range correlations at distances $R > R_p$ as the excitation time increases. The pair correlation function approaches the value of one in the range 15 μm $\lesssim R \lesssim R_c$, with a cutoff R_c that is given by the overall cloud size, and that increases in time. Due to the anisotropy of the excitation region, R_c also depends on azimuthal angle, as evident from the oblong shape of the pair correlation images in Fig. 1.

We note that in a related experiment [21] we have used the same preparation technique, but the excitation pulse duration was short and fixed (5 μs) while the interaction time was varied up to 40 μs. There, R_p increased due to the repulsive van der Waals interaction. Since in [21] the growing gaps between the Rydberg atoms did not become filled in with newly excited Rydberg atoms, the distance of the maximal correlation, R_p, was increasing in time. In contrast, in the present case the excitation pulse remains on, and the gaps between the Rydberg atoms become continually refilled. We find that R_p becomes time-independent because of that difference.

The dark pattern near the center of the pair correlation images in Figs. 1(a-d) and the small peak to the left

of the gray region in Figs. 1(e, f) originate from an ion feedback mechanism, as explained in [26, 29]. Any correlation within a radius $R_{\rm fb} \approx 5$ μm [see Figs. 1(e, f)] is, in most instances, not real and likely due to the ion feedback. This results in double counting of some Rydberg atoms. We correct this experimental artifact by replacing any pair of ions detected at a distance $\leq R_{\rm fb}$ with a single ion located at the average position of the ion pair. In our experimental data, the secondary ions account for about 8% of the total number of detections. In the remainder of this paper, the numbers and positions of the Rydberg atoms are corrected in this manner.

IV. RYDBERG CLOUD DISTRIBUTION

After having found that the continual excitation has observable effects in the short-range correlations, we now study the overall expansion dynamics of the Rydberg-atom clouds. We obtain averaged Rydberg-atom-cloud distributions by accumulating 10000 images [see inset of Fig. 2(a)], and integrating the number of counts along the y-axis. The distributions of the Rydberg atom clouds for $\Delta = 0$ at various excitation durations are shown in Fig. 2(a). For a $5-\mu$s pulse duration the distribution of the cloud is expected to be Gaussian, as it should mimic the shape of the excitation laser. At longer excitation durations the distribution grows in height and width. The distribution keeps growing in height because of the ongoing production of Rydberg atoms within the excitation region, which also causes the central portion of the whole curve to still resemble the Gaussian beam shape. The distribution also grows in width because of the initial thermal velocity of the atoms and the repulsive van der Waals pressure, which cause the atoms to stream out and move away from the excitation region.

In addition to the overall expansion dynamics, it is of interest in how far initially present correlations between Rydberg atoms, generated in the course of photoexcitation, persist through the expansion process. In each of the above 10000 images, we extract subsamples that contain primarily pair-correlated atoms by selecting atoms with a separation between 5 and 15 μm [shaded region in Figs. 1(e, f)]. Within this range of the interatomic separation, for $\Delta = 4$ MHz the excitation is enhanced due to the matching between the van der Waals interaction of neighboring atoms and the laser detuning. We also perform the same type of subsampling for $\Delta = 0$ case. The total distribution and the distribution of the subsamples of pair-correlated atoms are compared in Fig. 2(b, c) for two different pulse durations. For the 5-μs pulse duration, the correlated-atom distribution is about the same as the total distribution.

For the 320-μs pulse duration, the total and correlated-atom distributions are both significantly wider than those of the 5 μs pulse, as already seen in Fig. 2(a), but quite different in shape. The width of the correlated-atom distribution does not increase as rapidly as that of the total distribution. Hence, in the outer regions of the evolved atom distribution there is a relative deficiency of pair correlations at radii R between 5 and 15 μm. Data equivalent to Fig. 2(c), taken for different times, indicate that the timescale over which this deficiency develops is in the range of 50-100 μs. This is on the same order as the timescale over which the van der Waals repulsion between atom pairs removes correlations (40 μs; see Ref. [21]). Hence, the van der Waals pressure is responsible for both the overall expansion dynamics as well as the lack of correlations in the outer region of the evolved atom clouds.

It is somewhat unexpected that in Fig. 2(c) at times $\gtrsim 40$ μs and positions $\gtrsim 20$ μm the fraction of pair-correlated atoms apparently is still substantial. Following the discussion in the previous paragraph, and considering the fact that the detection is a 2-dimensional projection of a 3-dimensional excitation region, these pair correlations must be mostly accidental, *i.e.*, due to atoms that are out-of-plane but happen to be close to each other on the projection. A secondary reason may be that, in the fringes of the optical excitation region, atoms streaming out of the excitation region still lead to some facilitated excitations along their trajectories. We have repeated the analysis presented in Figs. 2(a-c) for the case $\Delta = 4$ MHz and observed the same qualitative behavior. There is a difference in that the width of the atom distributions for $\Delta = 4$ MHz is generally smaller than for $\Delta = 0$ MHz. This is due to the smaller number of Rydberg atoms in the $\Delta = 4$ MHz case, which results in a reduced overall van der Waals pressure.

The picture that may be drawn from the previous discussion is that the atom sample should consist of two populations: an evolved population generated by the ongoing conversion of electrostatic energy of the many-body Rydberg system (van der Waals interaction energy) into kinetic energy, and a population consisting of newly excited atoms. The atoms belonging to the evolved population are relatively fast and stream out of the excitation region, reaching distances that grow with excitation-pulse duration. The evolved population exhibits only a small degree of enhanced pair correlation near $R_{\rm p}$. The new population is concentrated in the excitation region, those atoms are relatively slow, and their degree of enhanced pair correlation near $R_{\rm p}$ is large. The presence of two types of populations motivates us to fit the data in Fig. 2(a), as well as analogous data for $\Delta = 4$ MHz, with double-Gaussians

$$G(x) = A \exp\left[\frac{(x-x_{\rm c})^2}{2\sigma_{\rm A}^2}\right] + B \exp\left[\frac{(x-x_{\rm c})^2}{2\sigma_{\rm B}^2}\right] \quad , \quad (1)$$

where the first term is for the new and the second term is for the evolved population, A and B are the respective weights, $\sigma_{\rm A}$ and $\sigma_{\rm B}$ are the standard deviations attributed to the two populations, and $x_{\rm c}$ is the center, which is taken to be the same for both distributions. We fix $\sigma_{\rm A}$ because it carries the geometric property of the excitation region. Here, $\sigma_{\rm A} = 5.84$ μm for $\Delta = 0$ and $\sigma_{\rm A} = 4.78$ μm for $\Delta = 4$ MHz. These values are obtained from single-Gaussian fits of the data for the 5-μs pulse duration. The total and pair-correlated distribu-

tions have about the same σ_A, as seen in Fig. 2(b). The σ_A-values are just slightly larger than $w_0/2$ of the excitation beam, as expected.

Figures 2(d, e) show the values for σ_B for both the total and pair-correlated distributions. Gray symbols represent data that can be modeled well using a single-Gaussian fit. Using a double-Gaussian fit on such data results in small and erratic amplitudes B, with $B \lesssim 0.1...0.01A$, as well as unreasonably large values of σ_B. Therefore, the gray symbols in Fig. 2(d, e) are ignored. We calculate the expansion velocity of the distributions by performing a linear fit to $\sigma_B(t)$ over the pulse-duration range 40 to 160 μs, in which the expansion velocity is approximately constant. We exclude the points at 320 μs because the atom distribution becomes truncated by the limited field of view [see Fig. 2(a, c) at 320 μs]. The truncation leads to σ_B-values that are too small at the latest times.

From Figs. 2(d, e) it can be seen that the expansion velocity of the $\Delta = 0$ case is higher than that of the $\Delta = 4$ MHz case. This is because there are more atoms excited in the $\Delta = 0$ than in the $\Delta = 4$ MHz case [see Fig. 3(b)]. The overall van der Waals pressure for $\Delta = 0$ is then larger than for $\Delta = 4$ MHz. It is noted that, in both cases, the atoms have a lower velocity than if they were excited with a short excitation pulse [21], where the Rydberg atoms reach a terminal velocity of 0.18 m/s after about 20 μs. This velocity is about 3 times larger than the expansion velocity of the cloud distribution observed in this work. This difference arises from the fact that in Ref. [21] we have studied the repulsion of Rydberg-atom pairs selectively prepared at a small initial internuclear separation, whereas the present experiment reveals the (slower) mean-field expansion. The expansion velocities in Figs. 2(d, e) are on the same order as the initial thermal velocity, which is ≈ 0.1 m/s. However, the expansion reflects a directed outward motion, whereas the thermal velocity distribution is random, with an average of zero.

V. COUNTING STATISTICS

We now turn to study the effect of excitation pulse durations and detunings on the counting statistics of Rydberg atoms, which is known to exhibit sub-Poissonian character or bimodality, depending on conditions [22, 23]. In each dataset, we extract the number of detected Rydberg atoms after removing ion feedback (see Section III). The number distributions of detected Rydberg atoms, obtained from 10000 samples recorded for various pulse durations and detunings, are shown in Fig. 3(a). For $\Delta = 0$ each dataset is fit well by a Poissonian distribution, with averages denoted $\langle n_0 \rangle$. For $\Delta = 4$ MHz, at short excitation times the distribution has one peak, while at excitation durations greater than 40 μs it is bimodal. Therefore, for $\Delta = 4$ MHz we apply a double-Poissonian fit,

$$P(k) = C_1 \frac{\langle n_1 \rangle^k e^{-\langle n_1 \rangle}}{k!} + C_2 \frac{\langle n_2 \rangle^k e^{-\langle n_2 \rangle}}{k!} \quad , \qquad (2)$$

where C_1 and C_2 are weighting factors with $C_1 + C_2 = 1$, and $\langle n_1 \rangle$ and $\langle n_2 \rangle$ are the corresponding averages, where $\langle n_1 \rangle < \langle n_2 \rangle$. Also, k is the number of detected Rydberg atoms in each image. As seen in Fig. 3(a), the fits match the histograms very well.

In Fig. 3(b) we show the fitted averages, $\langle n_0 \rangle$ for $\Delta = 0$ and $\langle n_1 \rangle$, $\langle n_2 \rangle$ for $\Delta = 4$ MHz, with the areas of the circles representing the respective weighting factors, C_1 and C_2. For $\Delta = 0$, the average number of excitation increases and reaches a value of about 14 atoms at the longest excitation time. For $\Delta = 4$ MHz and pulse durations less than 20 μs, $C_1 > C_2$ (red circles are bigger than blue circles), *i.e.,* the Poissonian component with the smaller average, $\langle n_1 \rangle$, carries the stronger weight. For longer pulse durations, $C_1 < C_2$, *i.e.,* the Poissonian with the larger average, $\langle n_2 \rangle$, carries the stronger weight.

We interpret the observed time-dependence of the weighting factors C_1 and C_2 as follows. At early times, the Rydberg atom sample consists of off-resonantly excited single atoms or atom pairs in close proximity with each other, as explained in Section III. These form the Poissonian with the smaller average $\langle n_1 \rangle$. As time proceeds, each atom or atom pair tends to act as a "seed" for subsequent facilitated excitations in its vicinity, giving rise to the Poissonian with the larger average $\langle n_2 \rangle$. Both the values of $\langle n_2 \rangle$ and C_2 are increasing in time; at times $\gtrsim 80$ μs the Poissonian with the large average becomes dominant. This is interpreted as the facilitation process gaining traction at those later times, in almost all realizations of the experiment.

VI. MANDEL Q-PARAMETER

A parameter that is widely used to characterize the correlations of the system is the Mandel Q-parameter [10, 22, 23, 30]

$$Q = \frac{\langle n(\tau_p)^2 \rangle - \langle n(\tau_p) \rangle^2}{\langle n(\tau_p) \rangle} - 1 \quad . \qquad (3)$$

Figure 3(c) shows the Q-parameter as a function of excitation duration τ_p and detuning of the continuously excited Rydberg-atom system. For $\Delta = 0$, the Q-value decreases as the excitation duration increases, indicating that the system acquires sub-Poissonian character ($Q < 0$), a fact that is well-known [10, 22, 23]. Here, we also find that the system maintains an approximately constant, negative Q-value out to an excitation duration of 320 μs. Conversely, for $\Delta = 4$ MHz the system develops a super-Poissonian character ($Q > 0$) [14, 29, 31] that persists through the maximum experimentally probed excitation duration.

VII. CONCLUSION

In summary, we have observed the behavior of a continuously excited Rydberg-atom system in the blockaded and facilitated regimes. We have focused on how pair correlations, the excitation number distribution, and the counting statistics behave on timescales that exceed the Rydberg-atom decay time and timescale on which the

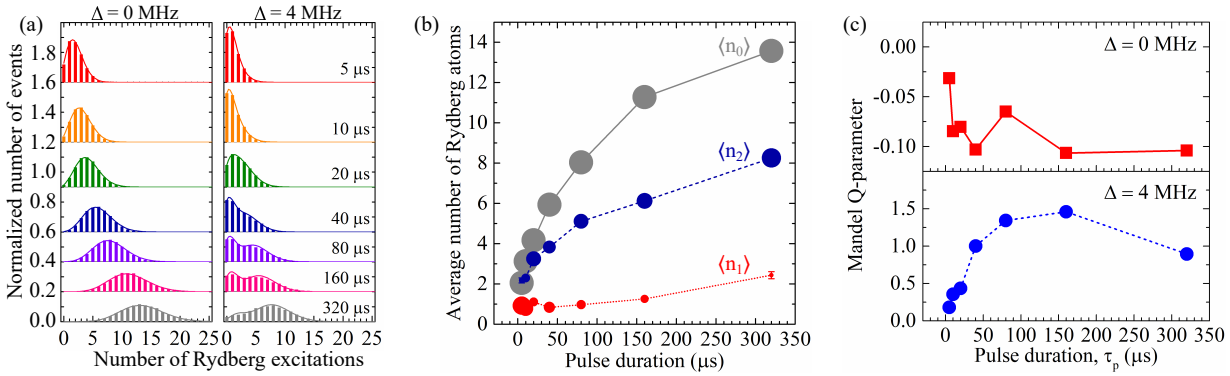

FIG. 3. (a) Histograms of the number of detected Rydberg atoms for $\Delta = 0$ MHz with unimodal Poissonian fit and $\Delta = 4$ MHz with bimodal Poissonian fit (Eq. 2). (b) Average numbers $\langle n_i \rangle$ of Rydberg atoms as a function of excitation pulse duration τ_p. Gray circles and the solid line are for $\Delta = 0$ MHz ($\langle n_0 \rangle$). Colored circles are for $\Delta = 4$ MHz. The red circles with the dotted line correspond to $\langle n_1 \rangle$, and the blue circles with the dashed line to $\langle n_2 \rangle$ (the lines are to guide the eye). Circle areas are proportional to the respective weighting factors C_1 and C_2 (see Eq. 2). Uncertainty bars are smaller than the symbol size for most cases. (c) Mandel Q-parameter for $\Delta = 0$ and 4 MHz vs τ_p.

potential energy of the photoexcited system becomes converted into kinetic energy. Our results are relevant to the understanding of many-body effects in such systems, including the specific role of the continual excitation [13, 32]. A large number of physical processes are important in this continuously pumped Rydberg-atom system, including radiative black-body transitions, energy-exchanged collisions, ionization, and collisions between Rydberg atoms and charged particles. Due to the complexity of the ensuing dynamics, more experimental and theoretical work is anticipated to fully understand the system. Our work may lead to future studies along these lines.

ACKNOWLEDGMENTS

This work was supported by the NSF Grant No. PHY-1506093 and the AFOSR Grant No. FA9550-10-1-0453. N.T. acknowledges support from DPST of Thailand.

* nithi@umich.edu
† Present address: Physikalisches Institut, Universität Heidelberg, Im Neuenheimer Feld 226, 69120 Heidelberg, Germany
†† Present address: Terumo Heart, Inc., Ann Arbor, Michigan 48103, USA

[1] M. Saffman, T. G. Walker, and K. Mølmer, Rev. Mod. Phys. **82**, 2313 (2010).
[2] R. Löw, H. Weimer, J. Nipper, J. B. Balewski, B. Butscher, H. P. Büchler, and T. Pfau, J. Phys. B: At. Mol. Opt. Phys. **45**, 113001 (2012).
[3] P. Pillet and T. F. Gallagher, J. Phys. B: At. Mol. Opt. Phys. **49**, 174003 (2016).
[4] J. Sanders, M. Jonckheere, and S. Kokkelmans, Phys. Rev. Lett. **115**, 043002 (2015).
[5] R. Gutiérrez, C. Simonelli, M. Archimi, F. Castellucci, E. Arimondo, D. Ciampini, M. Marcuzzi, I. Lesanovsky, and O. Morsch, Phys. Rev. A **96**, 041602 (2017).
[6] T. Pohl, E. Demler, and M. D. Lukin, Phys. Rev. Lett. **104**, 043002 (2010).
[7] R. M. W. v. Bijnen, S. Smit, K. A. H. v. Leeuwen, E. J. D. Vredenbregt, and S. J. J. M. F. Kokkelmans, J. Phys. B: At. Mol. Opt. Phys. **44**, 184008 (2011).
[8] P. Schauß, J. Zeiher, T. Fukuhara, S. Hild, M. Cheneau, T. Macrì, T. Pohl, I. Bloch, and C. Gross, Science **347**, 1455 (2015).
[9] M. Gärttner, K. P. Heeg, T. Gasenzer, and J. Evers, Phys. Rev. A **88**, 043410 (2013).
[10] H. Schempp, G. Günter, M. Robert-de Saint-Vincent, C. S. Hofmann, D. Breyel, A. Komnik, D. W. Schönleber, M. Gärttner, J. Evers, S. Whitlock, and M. Weidemüller, Phys. Rev. Lett. **112**, 013002 (2014).
[11] A. Urvoy, F. Ripka, I. Lesanovsky, D. Booth, J. P. Shaffer, T. Pfau, and R. Löw, Phys. Rev. Lett. **114**, 203002 (2015).
[12] C. Ates, T. Pohl, T. Pattard, and J. M. Rost, Phys. Rev. A **76**, 013413 (2007).
[13] M. M. Valado, C. Simonelli, M. D. Hoogerland, I. Lesanovsky, J. P. Garrahan, E. Arimondo, D. Ciampini, and O. Morsch, Phys. Rev. A **93**, 040701 (2016).
[14] K. P. Heeg, M. Gärttner, and J. Evers, Phys. Rev. A **86**, 063421 (2012).
[15] D. Tong, S. M. Farooqi, J. Stanojevic, S. Krishnan, Y. P. Zhang, R. Côté, E. E. Eyler, and P. L. Gould, Phys. Rev. Lett. **93**, 063001 (2004).
[16] M. Gärttner, K. P. Heeg, T. Gasenzer, and J. Evers, Phys. Rev. A **86**, 033422 (2012).
[17] R. Heidemann, U. Raitzsch, V. Bendkowsky, B. Butscher, R. Löw, L. Santos, and T. Pfau, Phys. Rev. Lett. **99**, 163601 (2007).
[18] C. Ates and I. Lesanovsky, Phys. Rev. A **86**, 013408

(2012).
[19] R. Faoro, C. Simonelli, M. Archimi, G. Masella, M. M. Valado, E. Arimondo, R. Mannella, D. Ciampini, and O. Morsch, Phys. Rev. A **93**, 030701 (2016).
[20] S. Möbius, M. Genkin, S. Wüster, A. Eisfeld, and J. M. Rost, Phys. Rev. A **88**, 012716 (2013).
[21] N. Thaicharoen, A. Schwarzkopf, and G. Raithel, Phys. Rev. A **92**, 040701 (2015).
[22] T. Cubel Liebisch, A. Reinhard, P. R. Berman, and G. Raithel, Phys. Rev. Lett. **95**, 253002 (2005).
[23] N. Malossi, M. M. Valado, S. Scotto, P. Huillery, P. Pillet, D. Ciampini, E. Arimondo, and O. Morsch, Phys. Rev. Lett. **113**, 023006 (2014).
[24] P. Schauß, M. Cheneau, M. Endres, T. Fukuhara, S. Hild, A. Omran, T. Pohl, C. Gross, S. Kuhr, and I. Bloch, Nature **491**, 87 (2012).
[25] A. Schwarzkopf, D. A. Anderson, N. Thaicharoen, and G. Raithel, Phys. Rev. A **88**, 061406 (2013).
[26] N. Thaicharoen, L. Gonçalves, and G. Raithel, Phys. Rev. Lett. **116**, 213002 (2016).
[27] A. Reinhard, T. C. Liebisch, B. Knuffman, and G. Raithel, Phys. Rev. A **75**, 032712 (2007).
[28] T. M. Weber, M. Höning, T. Niederprüm, T. Manthey, O. Thomas, V. Guarrera, M. Fleischhauer, G. Barontini, and H. Ott, Nat Phys **11**, 157 (2015).
[29] N. Thaicharoen, A. Schwarzkopf, and G. Raithel, Phys. Rev. Lett. **118**, 133401 (2017).
[30] C. Ates, T. Pohl, T. Pattard, and J. M. Rost, J. Phys. B: At. Mol. Opt. Phys. **39**, L233 (2006).
[31] S. Wüster, J. Stanojevic, C. Ates, T. Pohl, P. Deuar, J. F. Corney, and J. M. Rost, Phys. Rev. A **81**, 023406 (2010).
[32] F. Letscher, D. Petrosyan, and M. Fleischhauer, New J. Phys. **19**, 113014 (2017).